Magnetic Resonance in Medicine 44:450–456 (2000)

$H_2{}^{15}O$ PET Validation of Steady-State Arterial Spin Tagging Cerebral Blood Flow Measurements in Humans

Frank Q. Ye,[1] Karen Faith Berman,[1] Timothy Ellmore,[1] Giuseppe Esposito,[1] John D. van Horn,[1] Yihong Yang,[2] Jeff Duyn,[2] Anne M. Smith,[2] Joseph A. Frank,[2] Daniel R. Weinberger,[1] and Alan C. McLaughlin[1]*

Steady-state arterial spin tagging approaches can provide quantitative images of CBF, but have not been validated in humans. The work presented here compared CBF values measured using steady-state arterial spin tagging with CBF values measured in the same group of human subjects using the $H_2{}^{15}O$ IV bolus PET method. Blood flow values determined by $H_2{}^{15}O$ PET were corrected for the known effects of incomplete extraction of water across the blood brain barrier. For a cortical strip ROI, blood flow values determined using arterial spin tagging (64 ± 12 cc/100g/min) were not statistically different from corrected blood flow values determined using $H_2{}^{15}O$ PET (67 ± 13 cc/100g/min). However, for a central white matter ROI, blood flow values determined using arterial spin tagging were significantly underestimated compared to corrected blood flow values determined using $H_2{}^{15}O$ PET. This underestimation could be caused by an underestimation of the arterial transit time for white matter regions. Magn Reson Med 44:450–456, 2000. Published 2000 Wiley-Liss, Inc.†

Key words: PET; arterial spin tagging; CBF; $H_2{}^{15}O$; MRI

Steady-state MR arterial spin tagging approaches (1,2) can image resting cerebral blood flow (CBF) in humans (3–6), and have been used to follow CBF increases during motor (7,8) and cognitive (9) tasks, and CBF decreases in cerebrovascular disease (10).

One of the advantages of steady-state spin tagging approaches is the ability to provide quantitative images of CBF measured in classical physiological units (i.e., cc/100g/min). However, a number of potential artifacts could compromise the accuracy of calculated CBF values. One set of artifacts arises from magnetization transfer effects (11). Another set of artifacts arises from vascular effects; e.g., transit delays in tagged blood reaching the capillary exchange site, and the presence of tagged water in the arterial bed (6,12).

One way to investigate the accuracy of arterial spin tagging is to compare CBF values determined using this approach with CBF values determined using a "gold standard." In the rat, CBF values measured using arterial spin tagging agree well with CBF values measured simultaneously using radioactive microspheres (13). However, conclusions based on the rat model may not apply to humans, where many of the artifacts are substantially larger (6). The work described here investigates the accuracy of arterial spin tagging approaches for human studies by comparing CBF values measured using arterial spin tagging with CBF values measured in the same group of subjects using $H_2{}^{15}O$ positron emission tomography (PET).

MATERIALS AND METHODS

Experimental Protocol

Experiments were performed on 12 normal human subjects (5 males, average age = 38 ± 9 years; 7 females, average age = 38 ± 8 years) using a protocol approved by the Institutional Review Board of the National Institute of Mental Health.

Arterial spin tagging approaches were used to obtain a 2D image of resting CBF values in a 5-mm axial slice placed approximately 2 cm above the corpus callosum. In a separate experiment (on a different day) $H_2{}^{15}O$ PET was used to measure resting CBF values in the same subject. A slice in the $H_2{}^{15}O$ PET CBF image that corresponded to the slice used for the MR CBF image was selected, and the blood flow images of this slice were compared across the two techniques.

Magnetic Resonance Imaging

All MR experiments were performed on a Signa 1.5 T (General Electric, Milwaukee, WI) scanner using a standard quadrature head coil and a standard body-gradient coil capable of a maximum amplitude of 22 milliTesla/meter (mT/m) and a maximum slew rate of 120 Tesla/meter/second. Anatomical MR images were acquired as a series of 124 sagittal sections using a 3D spoiled gradient echo (SPGR) sequence with the following parameters: matrix = 128 × 256, slice thickness = 1.5 mm, TE = 5 msec, TR = 24 msec, and flip angle = 45°.

Perfusion images were obtained using single-shot 2D spin-echo SPIRAL approaches (14). Images were obtained with: matrix = 96 × 96, FOV = 24 cm, slice thickness = 5 mm, TE = 19 msec, TR = 4.7 sec. The *k*-space data were zero-filled to a 128 × 128 matrix before image reconstruction. A fat-saturation pulse, consisting of a 16-msec nonselective sinc pulse followed by gradient spoiler pulses, was added to the sequence before the 90° excitation pulse. The length of the SPIRAL waveform was 40 msec. Symmetrical gradients (5.4 msec, 22 mT/m) were placed immediately before and after the 180° pulse to "crush" the signal from arterial water spins (6).

T_1 relaxation rates in the absence (R_{1o}) and the presence ($R_1(\omega_1,\Delta\omega)$) of off-resonance RF irradiation were deter-

[1]Clinical Brain Disorders Branch, National Institute of Mental Health, National Institutes of Health, Bethesda, Maryland.

[2]Laboratory of Diagnostic Radiology Research, Clinical Center, National Institutes of Health, Bethesda, Maryland.

*Correspondence to: Dr. Alan McLaughlin, Building 10, Room B1D-69, National Institutes of Health, 9000 Rockville Pike, Bethesda, MD 20892.

Received 29 June 1999; revised 17 November 1999; accepted 27 December 1999.

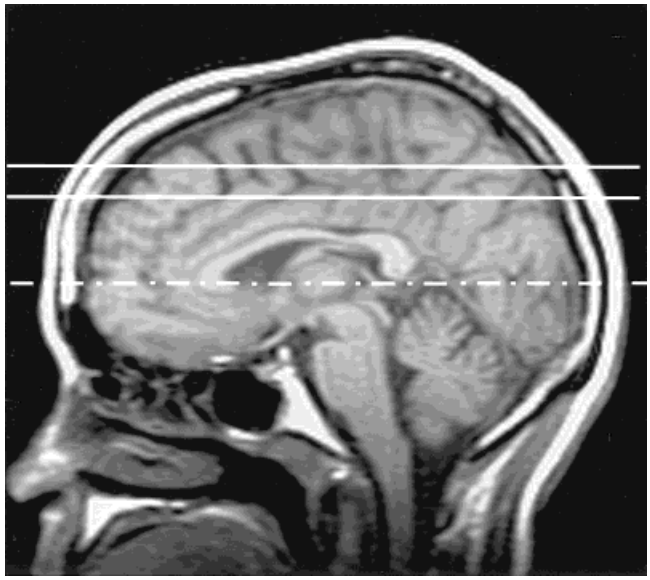

FIG. 1. Sagittal image of a human head, showing the approximate location of the imaging slice (solid lines) and the inversion plane (dashed line) used for the arterial spin tagging experiments.

mined for each voxel in the SPIRAL image using procedures described previously (6).

Flow-induced adiabatic inversion (2) was used to invert arterial water spins flowing through the tagging plane, which was placed 3 cm below the center of the imaging slice (see Fig. 1). Inversion was accomplished using a 3.5-sec off-resonance RF pulse train in the presence of a z gradient. The pulse train consisted of rectangular RF pulses of 75 msec duration separated by 10 msec. The amplitude of the off-resonance RF field (γB_1) was 170 Hz. This value was chosen because previous studies suggested that it produced maximum inversion of arterial water spins at the tagging plane under our conditions (4). The frequency offset of the irradiating RF field (± 6000 Hz) and the sign of the z gradient (± 4.8 mT/m) were alternated in a four-step protocol to minimize the influence of asymmetric magnetization transfer effects and gradient eddy currents (11). Each perfusion image was calculated using the data collected in a single four-pulse protocol (see below). The data collection time for a single four-pulse protocol was 18.8 sec. Data from ninety-six four pulse cycles were acquired, giving a total acquisition time of 30 min.

Arterial spin tagging data were acquired using a delayed acquisition approach (5). In this approach a delay, τ_{delay}, was inserted between the end of the tagging period and the beginning of the acquisition of the SPIRAL image. Crusher gradients were used to reduce the signal from tagged arterial blood, and CBF values (Q) were calculated with a one-compartment model, using the following equation (7)

$$\frac{\Delta M(\tau_{delay})}{M_o} = -\frac{2\alpha_o Q/\lambda}{R_{1o}} e^{-R_{1o}\tau_{delay}}\{1 - \psi_1 - \psi_2\}\{\psi_3\} \quad [1]$$

where

$$\psi_1 = \left(1 - \frac{R_{1o}}{R_1(\omega_1, \Delta\omega)}\right) e^{-R_{1o}\tau_a}, \quad [2]$$

$$\psi_2 = \frac{R_{1o}}{R_1(\omega_1, \Delta\omega)} e^{-[R_{1o}-R_1(\omega_1,\Delta\omega)]\tau_a} e^{-R_1(\omega_1,\Delta\omega)\tau_o}, \quad [3]$$

$$\psi_3 = e^{[R_{1o}-R_{1a}]\tau_a}, \quad [4]$$

and $\Delta M(\tau_{delay})$ is the difference in MR signal amplitude observed in the presence and absence of arterial tagging, M_o is the equilibrium value of the MR signal amplitude, R_{1a} is the relaxation rate of arterial water protons, τ_o is the length of the off-resonance RF irradiation, α_o is the extent of inversion of arterial water in the tagging plane, λ is the brain/blood partition coefficient and τ_a is the arterial transit time, i.e., the time for blood to move from the tagging plane to the capillary exchange site (6). Equation [1] assumes that τ_{delay} is longer than τ_a. λ was assumed to be 0.90 ml/g (15), R_{1a} was assumed to be 0.8 s^{-1}, τ_a was assumed to be 0.95 sec, and α_o was assumed to be 0.88 (6). τ_{delay} = 1.1 sec and τ_o = 3.5 sec. The use of a 90° excitation pulse made it unnecessary to correct for incomplete recovery of longitudinal magnetization during each TR cycle (6).

The voxel size for the 128 × 128 CBF images was 1.9 mm × 1.9 mm. CBF images were convolved with a 2D Gaussian kernel having a full-width-at-half-maximum (FWHM) of 3.8 mm. The FWHM of the point spread function for the convolved CBF images was approximately 5.5 mm. Initial CBF images were obtained with higher spatial resolution than the final convolved CBF images for two reasons: first, to match the 128 × 128 $H_2{}^{15}O$ PET data sets; second, to minimize the effects of heterogeneity in tissue R_{1o} values on the calculated CBF values (see Eq. [1]).

$H_2{}^{15}O$ PET Imaging

PET data were acquired on a Scanditronix PC2048-15B head tomograph which simultaneously produced 15 6.5-mm-thick contiguous slices per scan. Each slice was composed of a 128 × 128 matrix. In-plane and z axis spatial resolution (FWHM) was 6.0–6.5 mm after reconstruction. A thermoplastic mask was individually molded to each subject to immobilize the head, and scans were oriented parallel to the canthomeatal line. Transmission scans, collected by rotating a gallium-68/germanium-68 pin source about the head, were used to correct for attenuation of radiation by skull and brain tissue. Each subject had four emission scans, which were separated by a 12-min period to allow for decay of residual radiation. The average standard deviation of the four sequential measurements was ~7%. A bolus intravenous injection of 40–46 mCi of $H_2{}^{15}O$ preceded each emission scan. Emission data for each scan were acquired for 4 min in 16 frames (12 frames of 10 sec each, followed by 4 frames of 30 sec each), and were reconstructed with a Hanning filter using corrections for attenuation, scatter, random coincidences, and dead time.

Arterial input functions were measured using automated arterial blood sampling, with a continuous withdrawal rate of 3.8 ml/min. Coincident events were counted at 1-sec intervals by paired sodium iodide detectors, and

corrected for random coincidences, deadtime, and dispersion (16). Time shifts between scanner count rate and arterial count rate were determined in a manner similar to that described by Iida et al. (17). The arterial time-activity curve was used with a pixel-by-pixel least-squares fit for CBF and partition coefficient to produce quantitative CBF images (18).

Registration of MR CBF Images and PET CBF Images

Each of the four resting 15-slice $H_2{}^{15}O$ CBF images for an individual subject was aligned to the mean of the $H_2{}^{15}O$ CBF images using a six parameter (rigid body) registration algorithm (19). The four registered images were combined to create a new mean $H_2{}^{15}O$ PET CBF image for each subject, which was registered to the high-resolution anatomical MR image of the same subject using a six-parameter algorithm (19).

A slice corresponding to the 2D arterial spin tagging CBF image was outlined on the anatomical MR image, and a 2D $H_2{}^{15}O$ PET CBF image of this slice was constructed from the co-registered 3D $H_2{}^{15}O$ PET CBF map. Sinc interpolation was used to minimize artifacts in the resliced images.

A five-parameter affine/fixed-determinant model was used to correct for slight misregistration and spatial distortion between the 2D arterial spin tagging image and the 2D slice in the high-resolution anatomical MR image. This model allowed for non-rigid spatial correction if the total area was preserved (19).

Gray Matter/White Matter Segmentation

Anatomical MR images of the slice were segmented using a histogram approach, based on image intensity. The total intensity range was divided into four regions: 0%–10%, 10%–50%, 50%–60%, 60%–100%. Voxels with intensities in the first and third regions were disregarded, voxels with intensities in the second region were assigned to gray matter, and voxels with intensities in the fourth region were assigned to white matter.

Even if the $H_2{}^{15}O$ PET CBF images and the arterial spin tagging CBF images could be registered precisely to the high-resolution anatomical MRI images, the CBF images would not be superimposed precisely on the anatomical MRI images, because of the different spatial resolution. Imprecise superposition will lead to imprecise segmentation of gray and white matter regions.

SPIRAL MR images were segmented according to T_1 values (6). Voxels with T_1 values below 720 msec were assigned to white matter, voxels with T_1 values between 850 msec and 1300 msec were assigned to gray matter, and other voxels were disregarded.

Segmentation masks were applied to CBF images that had no further spatial filtering; i.e., the FWHM of the point-spread function for the $H_2{}^{15}O$ PET images was ~6.5 mm, while the FWHM of the point-spread function for the arterial spin tagging images was ~5.5 mm (see above).

Voxel by Voxel Comparison of CBF Images

$H_2{}^{15}O$ PET CBF images were convolved with a Gaussian kernel with a FWHM of 5.5 mm, and arterial spin tagging CBF images were convolved with a Gaussian kernel with a FWHM of 6.5 mm. The FWHM of the convolved point-spread functions were thus the same (8.5 mm) for the two CBF images.

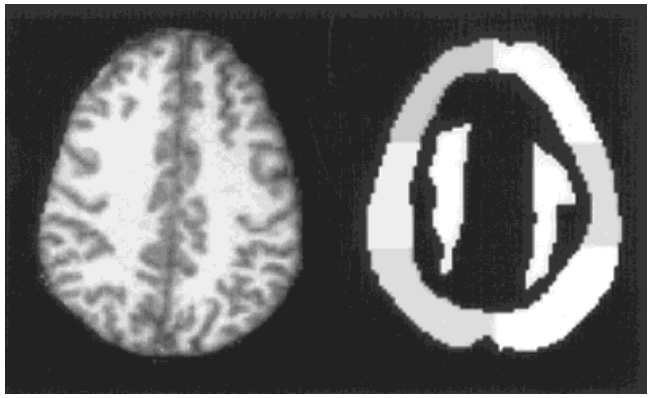

FIG. 2. Delineation of the cortical strip region of interest (ROI) and the white matter ROIs. The cortical strip ROI was subdivided into six ROIs: right anterior, right middle, right posterior, left anterior, left middle, and left posterior.

Region of Interest (ROI) Analysis of CBF Images

CBF images were filtered to a FWHM of 8.5 mm (see above). A cortical strip was drawn by visual inspection of the anatomical MR image of the slice, and divided (see Fig. 2) into six approximately equal regions (right anterior, right middle, right posterior, left anterior, left middle, left posterior). In addition, right and left central white matter ROIs were also drawn by visual inspection of the anatomical MR image. Finally, a whole slice ROI was drawn using all of the brain voxels in the slice. The nine ROIs were used to analyze arterial spin tagging and $H_2{}^{15}O$ PET CBF images of the slice.

RESULTS

Comparison of CBF Images

Figure 3 shows quantitative CBF images obtained using $H_2{}^{15}O$ PET and arterial spin tagging. Both images were acquired from the same slice in the same subject (see Materials and Methods). The two images show similar areas of elevated flow in gray matter regions, and a voxel-by-voxel comparison of the data from the images shown in Fig. 3 shows qualitative agreement across the entire CBF range (Fig. 4). The two images can be quantitatively compared using two different approaches: a gray matter/white matter comparison using segmented MR images, and an ROI comparison.

Gray Matter/White Matter Comparison Using Segmented MR Images

Segmented anatomical images were used to define gray matter and white matter masks (see Materials and Methods), which were then mapped onto the arterial spin tagging and $H_2{}^{15}O$ PET CBF images. For the arterial spin tagging blood flow images, the average gray matter/white matter CBF ratio was 1.6 ± 0.2. For the $H_2{}^{15}O$ PET CBF

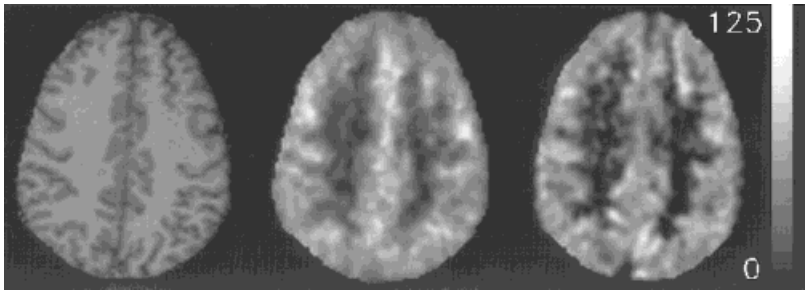

FIG. 3. Left: anatomical MR image of a 2D slice. Middle: quantitative CBF image of the slice obtained using $H_2{}^{15}O$ PET approaches. Right: quantitative CBF image of the same slice (in the same subject) obtained using steady-state arterial spin tagging approaches. The scale is in cc/100g/min. Data from subject #6.

images, the average gray matter/white matter CBF ratio was 1.4 ± 0.1. While the two ratios were similar, both were substantially lower than the expected ratio of gray matter/white matter blood flows (see Appendix A). This observation suggests that, using the procedures described here, superposition of the CBF images and the anatomical MR images was not precise enough to achieve good segmentation of gray and white matter regions (see Materials and Methods section), and this approach was not pursued.

ROI Comparison

F tests (ANOVA, $P = 0.05$) were performed to investigate variation in CBF values across the cortical strip ROIs (Fig. 2). No significant variation across the cortical strip ROIs was found for CBF values determined using arterial spin tagging approaches (Q_{AST}), for CBF values determined using $H_2{}^{15}O$ PET approaches (Q_{PET}), or for the difference between CBF values determined using the two approaches, i.e., Q_{AST}-Q_{PET}. The CBF data were thus averaged over the cortical strip ROIs. The average value of Q_{AST} for the combined cortical strip ROI was approximately 15% higher than the average value of Q_{PET} for the combined cortical strip ROI (paired t test, $P = 0.020$, $N = 12$) (see Table 1).

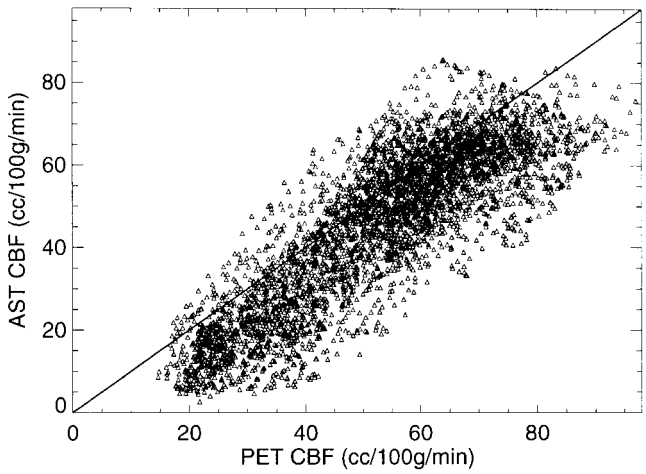

FIG. 4. Voxel-by-voxel comparison of the arterial spin tagging CBF image and the $H_2{}^{15}O$ PET CBF image of the same slice in the same subject (see Fig. 3). Data is taken from subject #6 (see Fig. 3). The images shown in Fig. 3 were convolved to bring the FWHM of the point spread function for each image to 8.5 mm (see Materials and Methods). Linear least squares analysis of the data gave a correlation coefficient (R) of 0.85. The solid line is the line of identity.

t tests ($P < 0.05$) were performed to investigate variation in CBF values between the right and left white matter ROIs. No significant right/left differences were found for Q_{AST}, Q_{PET} or Q_{AST}-Q_{PET}. The CBF data were thus averaged over the right and left white matter ROIs. For the combined white matter ROI there was a trend (paired t test, $P = 0.047$) for Q_{AST} to underestimate Q_{PET} by ~17% (see Table 1).

For the whole slice ROI there was a trend (paired t test, $P = 0.051$) for Q_{AST} to overestimate Q_{PET} by ~11% (see Table 1).

Table 1 also shows average values of F_{PET}, the corrected $H_2{}^{15}O$ CBF value (see Discussion). For the combined white matter ROI, the average value of Q_{AST} was approximately 30% lower than the average value of F_{PET} (paired t test, $P = 0.0007$).

DISCUSSION

Steady-state arterial spin tagging approaches can provide quantitative images of CBF (1,3–6), but have not been validated in humans. The major aim of the work presented here was to compare CBF values measured in humans using steady-state arterial spin tagging experiments (Q_{AST}) with CBF values measured in the same group of human subjects using $H_2{}^{15}O$ PET (Q_{PET}).

Table 1 shows that Q_{AST} values are approximately 15% larger than Q_{PET} values for the cortical strip ROI. The underlying reason for this discrepancy is not clear. Uncertainties in the exact value of the transit time, τ_a, could cause errors in Q_{AST}, but the delayed-acquisition approach used for these studies should substantially reduce the

Table 1
ROI Analysis of Cerebral Blood Flow Values

	Cortical strip (cc/100 g/min)	White matter (cc/100 g/min)	Whole slice (cc/100 g/min)
$\langle Q_{AST} \rangle$	64 ± 12	23 ± 8	55 ± 10
$\langle Q_{PET} \rangle$	56 ± 11*	27 ± 3	49 ± 8
$\langle F_{PET} \rangle$	67 ± 13	33 ± 4*	59 ± 10

$\langle Q_{AST} \rangle$ is the average cerebral blood flow value determined by arterial spin tagging approaches for the designated ROI. $\langle Q_{PET} \rangle$ is the average apparent cerebral blood flow value determined by $H_2{}^{15}O$ PET approaches for the designated ROI. $\langle F_{PET} \rangle$ is the average corrected cerebral blood flow determined by $H_2^{15}O$ PET approaches using Eq. [5].

*Denotes a statistically significant difference compared to Q_{AST} (paired t test, $N = 12$, $P \leq 0.02$).

magnitude of these errors for gray matter regions (5). Also, eddy-currents or asymmetric magnetization transfer effects could cause errors in Q_{AST}, but the four pulse protocol employed in these studies should minimize these errors (11).

Another explanation for the overestimation of Q_{AST} compared to Q_{PET} could be a systematic underestimation of CBF by the $H_2{}^{15}O$ PET approach, due to limitations in the exchange rate of water across the blood-brain barrier. A number of studies suggest that CBF values determined using $H_2{}^{15}O$ PET approaches are given by the following equation

$$Q_{PET} = EF, \quad [5]$$

where E is the extraction fraction of water, and F is the true CBF (20–23). Herscovitch et al. (22) demonstrated that E was reasonably uniform over the human brain (i.e., over white and gray matter), with an average value of 0.84 ± 0.07 under normocapnic conditions. Using this value of E in Eq. [5], corrected CBF values can be estimated from the observed values of Q_{PET}. Table 1 shows that CBF values determined for the cortical strip ROI using arterial spin tagging (Q_{AST}) agree very well with corrected CBF values determined using $H_2{}^{15}O$ PET and Eq. [5] (F_{PET}).

The $H_2{}^{15}O$ PET approach has other systematic errors apart from an underestimation of CBF due to the reduced extraction fraction (see Appendix B). However, the net effect of these other systematic errors should be relatively small, and should not alter the conclusions based on the results shown in Table 1 (see Appendix B).

Limitations in the exchange rate of water across the blood-brain barrier could also cause an underestimation of CBF values determined by arterial spin tagging approaches if tagged water in the vascular bed were crushed (24). However, given the slow velocities of water in the capillary bed, i.e., ~1 mm/sec (25), it is unlikely that the signal from tagged water in the capillary bed is crushed under the conditions used for our experiments, i.e., $b \sim 7$ s/mm^2 (26). If tagged water in the capillary bed is not crushed, a distributed model that includes the capillary bed suggests that CBF values determined using arterial spin tagging approaches are a good approximation to the corrected CBF, F (27).

Table 1 also shows that Q_{AST} values for the white matter ROI are ~30% lower than F_{PET} values determined using Eq. [5]. One explanation for the underestimation of white matter CBF values is related to the different arterial transit times (the time for tagged water to travel from the tagging plane to the capillary exchange site in the slice) for white matter and gray matter. Recent results suggest that white matter regions have longer arterial transit times than gray matter regions (28). The estimate for the transit time used in the present analysis (0.95 sec) was determined for gray matter regions (6), and could thus underestimate the arterial transit time for white matter regions. This underestimate in arterial transit time for white matter could produce a substantial underestimate in Q_{AST}. For example, if the white matter arterial transit time was double the observed gray matter arterial transit time, Q_{AST} for the white matter region would be underestimated by ~35%, which is consistent with the results shown in Table 1.

The study presented here illustrates some of the difficulties in comparing quantitative CBF images obtained using arterial spin tagging approaches with quantitative CBF images obtained using $H_2{}^{15}O$ PET approaches. One difficulty is superimposing the two CBF images. In the present study the 3D $H_2{}^{15}O$ PET CBF image was registered with a high-resolution 3D anatomical MR image. While this approach worked well enough to provide reasonable voxel-by-voxel correlation plots (see Fig. 4), it was not sufficiently precise to allow utilization of MR segmentation routines with the CBF images (see Appendix A). This limitation precluded a direct comparison of gray matter blood flows obtained using arterial spin tagging and $H_2{}^{15}O$ PET approaches. Instead, we compared CBF values in a cortical strip ROI.

The results presented in Table 1 raise possible questions concerning gray matter blood flow values determined by arterial spin tagging approaches. CBF values determined by arterial spin tagging approaches agree with corrected CBF values determined by $H_2{}^{15}O$ PET approaches for the cortical strip ROI (which contains contributions from gray and white matter), but underestimate corrected CBF values determined by $H_2{}^{15}O$ PET approaches for the white matter ROI. These observations bring up the possibility that arterial spin tagging approaches could overestimate gray matter CBF values. An analysis of the data shown in Table 1 suggests that this overestimation could be approximately 4% (see Appendix C).

Another difficulty in comparing arterial spin tagging and $H_2{}^{15}O$ PET approaches arises from the fact that, although both studies could be performed on the same subject, they could not be performed at the same time. This limitation introduced extra variance into the calculated CBF values due to inter-exam temporal variation. Previous studies suggest that the inter-exam variance in gray matter CBF values determined by arterial spin tagging is ~9% in experienced MR subjects (F. Ye et al., unpublished observations).

In summary, for a cortical strip ROI, steady-state arterial spin tagging approaches give CBF values that are not statistically different from corrected CBF values calculated using $H_2{}^{15}O$ PET approaches. However, for a white matter ROI, arterial spin tagging approaches substantially underestimate corrected CBF values determined by $H_2{}^{15}O$ PET approaches.

ACKNOWLEDGMENTS

We are grateful to Keith St. Lawrence and Peter Herscovitch for helpful discussions, and to Carlo Salustri for assistance with the pulse programming.

APPENDIX A

Segmentation Analysis of CBF Values

In the present study the segmentation analysis was performed on anatomical images obtained using a 128×256 SPGR sequence, while the arterial spin tagging blood flow image was obtained using a 96×96 SPIRAL sequence (see Materials and Methods). The data were analyzed in this manner so that a common segmentation map could be

Table 2
Segmentation Analysis of Cerebral Blood Flow Values

	"SPIRAL" segmentation	"Anatomical" segmentation
$\langle Q_{AST}^{grey} \rangle$	70 ± 11 cc/100 g/min	68 ± 12 cc/100 g/min
$\langle Q_{AST}^{white} \rangle$	25 ± 8 cc/100 g/min	43 ± 8 cc/100 g/min
$\langle Q_{AST}^{grey}/Q_{AST}^{white} \rangle$	2.9 ± 0.5	1.6 ± 0.2
$\langle Q_{PET}^{grey} \rangle$		58 ± 10 cc/100 g/min
$\langle Q_{PET}^{white} \rangle$		42 ± 6 cc/100 g/min
$\langle Q_{PET}^{grey}/Q_{PET}^{white} \rangle$		1.4 ± 0.1

$\langle Q_{AST}^{grey} \rangle$ and $\langle Q_{AST}^{white} \rangle$ are average grey matter and white matter blood flow values, respectively, measured using arterial spin tagging approaches. $\langle Q_{PET}^{grey} \rangle$ and $\langle Q_{PET}^{white} \rangle$ are average grey matter and white matter blood flows, respectively, measured using $H_2^{15}O$ PET approaches. "SPIRAL" segmentation used T_1 images acquired with SPIRAL MR techniques, while "Anatomical" segmentation used T_1 images acquired using standard anatomical MR techniques (see Materials and Methods).

used for arterial spin tagging and $H_2{}^{15}O$ PET CBF images. However, the different spatial resolution of the segmentation and CBF maps could affect the superposition of the two images, and reduce the observed gray matter/white matter blood flow ratio.

The effects of imprecise superposition can be investigated using T_1 images obtained with SPIRAL techniques to segment the arterial spin tagging CBF images (also obtained with SPIRAL techniques). Using this approach, the average gray matter/white matter blood flow ratio was ~2.9 (see Table 2). This value was substantially larger than the value obtained using anatomical images to segment arterial spin tagging blood flow images (~1.6, see Table 2).

The gray matter/white matter blood flow ratio obtained using segmentation maps derived from SPIRAL images cannot be considered an absolute measure of the average gray matter/white matter blood flow ratio, for two reasons. First, the present work suggests that arterial spin tagging approaches underestimate white matter blood flow by ~30% (see Discussion). Second, the finite spatial resolution will create intrinsic partial volume effects, which will cause an underestimate in the gray matter/white matter blood flow ratio.

APPENDIX B

Experimental Errors in $H_2{}^{15}O$ PET Measurements of CBF

Although $H_2{}^{15}O$ PET approaches have been used as a "gold standard" in the validation studies presented here, they themselves have a number of sources of error. Steady-state (29), autoradiographic (21) and dynamic (18,30) versions of the $H_2{}^{15}O$ PET experiment have somewhat different errors (18,31–34). This section outlines the major systematic and random errors in CBF values estimated using the dynamic $H_2{}^{15}O$ PET approach employed in this study (18).

The three major systematic errors are due to heterogeneity in brain composition, heterogeneity in tracer arrival time in the brain, and arterial blood contributions. Koeppe et al. [18,32] estimated that heterogeneity in brain composition could produce an underestimation of CBF by ~4% (18), while arterial blood contributions could produce an overestimation of CBF by ~7% (32). These two errors tend to counterbalance each other, and it is reasonable to assume that the net systematic error due to these two effects is less than ± 5%. Koeppe et al. [18] also estimated that heterogeneity in tracer arrival time could produce an error in CBF of approximately ± 5% (32).

The precision of CBF values calculated by dynamic $H_2{}^{15}O$ PET approaches can be estimated from the random variation observed in sequential measurements. In the studies reported here, the average standard deviation in a series of four CBF measurements (during the same exam) was ~7% (see Materials and Methods). Using this information, the random deviation of the $H_2{}^{15}O$ PET CBF values used in the present work (i.e., the average of the four sequential measurements) is estimated to be ~3.5%.

Assuming the systematic and random errors given above, the expected error in average CBF values calculated using $H_2{}^{15}O$ PET was estimated to be less than ± 7%. This is substantially smaller than the difference between $\langle Q_{PET} \rangle$ and $\langle Q_{AST} \rangle$ observed for the cortical strip ROI, or the difference between $\langle F_{PET} \rangle$ and $\langle Q_{AST} \rangle$ observed for the white matter ROI, in Table 1. This analysis suggests that conclusions based on the differences observed in Table 1 (see Discussion) are not affected by the major errors in the $H_2{}^{15}O$ PET measurements.

APPENDIX C

Analysis of Errors in Gray Matter CBF Values

Q_w and Q_g are defined as the white and gray matter CBF values. Q_w^{obx} and Q_g^{obs} are defined as the white and gray matter CBF values observed using arterial spin tagging approaches. $<Q>$ is defined as the average CBF value for the cortical strip ROI, and $<Q>^{obs}$ is defined as the observed average CBF value for the cortical strip ROI. With these definitions

$$\langle Q \rangle^{obs} = f_g Q_g^{obs} + f_w Q_w^{obs} \qquad [A1]$$

$$\langle Q \rangle = f_g Q_g + f_w Q_w, \qquad [A2]$$

where f_g and f_w are the gray matter and white matter fractions in the cortical strip ROI. Equations [A1] and [A2] can be rearranged to give

$$\frac{Q_g^{obs}}{Q_g} = \frac{\langle Q \rangle^{obs}}{\langle Q \rangle} + \frac{f_w}{f_g}\left(\frac{\langle Q \rangle^{obs}}{\langle Q \rangle} - \frac{Q_w^{obs}}{Q_w}\right)\frac{Q_w}{Q_g}. \qquad [A3]$$

Equation [A3] can be used to estimate the fractional error in gray matter CBF values calculated by arterial spin tagging approaches. $<Q>^{obs}$ is assumed to be equal to $<Q>_{AST}$ for the cortical strip ROI, $<Q>$ is assumed to be equal to $<F>_{PET}$ for the cortical strip ROI, Q_w^{obs} is assumed to be equal to $<Q>_{AST}$ for the white matter ROI, and Q_w is assumed to be equal to $<F>_{PET}$ for the white matter ROI. Using the values given in Table 1, Eq. [A3] becomes

$$\frac{Q_g^{obs}}{Q_g} = 0.95 + 0.25\,\frac{f_w}{f_g}\frac{Q_w}{Q_g} \qquad [A4]$$

If a value of f_w/f_g is assumed, then a value of Q_w/Q_g that is consistent with the data shown in Table 1 can be calculated using Eq. [A2]. For example, if f_w/f_g is assumed to be 1, Q_w/Q_g is calculated to be 0.33.

Using these values of f_g/f_w and Q_w/Q_g, Q_g/Q_g^{obs} is estimated to be 1.04. This calculation suggests that the arterial spin tagging approach could overestimate gray matter CBF values by approximately 4%.

REFERENCES

1. Detre JA, Leigh JS, Williams DS, Koretsky A. Perfusion imaging. Magn Reson Med 1992;23:37–45.
2. Williams DS, Detre JA, Leigh JS, Koretsky AP. Magnetic resonance imaging of perfusion using spin inversion of arterial water. Proc Nat Acad Sci USA 1992;89:212–216.
3. Roberts DA, Detre JA, Bolinger L, Insko, EK, Leigh JS. Quantitative magnetic resonance imaging of human brain perfusion at 1.5 T using steady-state inversion of arterial water. Proc Nat Acad Sci USA 1994; 91:33–37.
4. Ye FQ, Pekar JJ, Jezzard P, Duyn J, Frank JA, McLaughlin AC. Perfusion imaging of the human brain at 1.5 T using a single-shot EPI spin tagging approach. Magn Reson Med 1996;36:219–224.
5. Alsop DC, Detre JA. Reduced transit-time sensitivity in noninvasive magnetic resonance imaging of human cerebral blood flow. J Cereb Blood Flow Metab 1996;16:1236–1249.
6. Ye FQ, Mattay VS, Jezzard P, Frank JA, Weinberger DR, McLaughlin AC. Correction for vascular artifacts in cerebral blood flow values measured using arterial spin tagging techniques. Magn Reson Med 1997;37:226–235.
7. Ye FQ, Smith AM, Yang Y, Duyn J, Mattay VS, Ruttimann EU, Frank JA, Weinberger DR, McLaughlin AC. Quantitation of regional cerebral blood flow increases during motor activation: A steady-state arterial spin tagging study. Neuroimage 1997;6:104–112.
8. Ye FQ, Yang Y, Duyn J, Mattay VS, Frank JA, Weinberger DR, McLaughlin AC. Quantitation of regional cerebral blood flow increases during motor activation: a multislice, steady-state, arterial spin tagging study. Magn Reson Med 1999;42:404–407.
9. Ye FQ, Smith AM, Mattay VS, Ruttimann UE, Frank JA, Weinberger DR, McLaughlin AC. Quantitation of regional cerebral blood flow increases in prefrontal cortex during a working memory task: a steady-state arterial spin tagging study. Neuroimage 1998;8:44–49.
10. Detre JA, Alsop DC, Vives LR, Maccotta L, Teener JW, Raps EC. Noninvasive MRI evaluation of cerebral blood flow in cerebrovascular disease. Neurology 1998;50:633–641.
11. Pekar J, Jezzard P, Roberts DA, Leigh JS, Frank JA, McLaughlin AC. Perfusion imaging with compensation for asymmetric magnetization transfer effects. Magn Reson Med 1996;35:70–79.
12. Zhang W, Williams DS, Detre JA, Koretsky AP. Measurement of brain perfusion by volume-localized NMR spectroscopy using inversion of arterial water spins: accounting for transit time and cross-relaxation. Magn Reson Med 1992;25:362–371.
13. Walsh EG, Minematsu K, Leppo J, Moore SC. Radioactive microsphere validation of a volume localized continuous saturation perfusion measurement. Magn Reson Med 1994;31:147–153.
14. Yang Y, Glover GH, van Gelderen P, Mattay VS, Santha AKS, Sexton R, Ramsey NF, Moonen CTW, Weinberger DR, Frank JA, Duyn J. Fast 3D functional magnetic resonance imaging at 1.5 T with spiral acquisition. Magn Reson Med 1996;36:620–626.
15. Herscovitch P, Raichle ME. What is the correct value for the brain-blood partition coefficient for water? J Cereb Blood Flow Metab 1985; 5:65–69.
16. Daube-Witherspoon ME, Chon KS, Green SL, Carson RE, Herscovitch P. Factors affecting dispersion correction for continuous blood withdrawal and counting systems. J Nucl Med 1992;33:1010.
17. Iida H, Kanno I, Miura S, Murakami M, Takahashi K, Uemura K. Evaluation of regional differences of tracer appearance time in cerebral tissues using [^{15}O] water and dynamic positron emission tomography. J Cereb Blood Flow Metab 1988;8:285–288.
18. Koeppe RA, Holden JE, Ip WR. Performance comparison of parameter estimation techniques for the quantitation of local cerebral blood flow by dynamic positron computed tomography. J Cereb Blood Flow Metab 1985;5:224–234.
19. Woods RP, Grafton ST, Holmes CJ, Cherry SR, Mazziotta JC. Automated image registration: I. General methods and intrasubject, intramodality validation. J Comput Assist Tomogr 1998;22:141–154.
20. Eichling JO, Raichle ME, Grubb RL, Ter-Pogossian MM. Evidence of the limitations of water as a freely diffusible tracer in brain of the Rhesus monkey. Circ Res 1994;35:358–364.
21. Raichle ME, Martin WRW, Herscovitch P, Mintun MA, Markham J. Brain blood flow measured with intravenous $H_2{}^{15}O$. II. Implementation and validation. J Nucl Med 1983;24:790–798.
22. Herscovitch P, Raichle ME, Kilbourn MR, Welch MJ. Positron emission tomographic measurement of cerebral blood flow and permeability-surface area product of water using [^{15}O] water and [^{11}C] butanol. J Cereb Blood Flow Metab 1987;7:527–542.
23. Berridge MS, Adler LP, Nelson AD, Cassidy EH, Muzic RF, Bednarczyk EM, Miraldi F. Measurement of human cerebral blood flow with [^{15}O]butanol and positron emission tomography. J Cereb Blood Flow Metab 1991;11:707–715.
24. Silva AC, Zhang W, Williams DS, Koretsky AP. Estimation of water extraction fractions in rat brain using magnetic resonance measurement of perfusion with arterial spin labeling. Magn Reson Med 1997;37:58–68.
25. Pawlik G, Rackl A, Bing RJ. Quantitative capillary topography and blood flow in the cerebral cortex of cats: an in vivo microscopic study. Brain Res 1981;208:35–58.
26. Kennan RP, Gao J-H, Zhong J, Gore JC. A general model of microcirculatory blood flow effects in gradient sensitized MRI. Med Phys 1994; 21:539–545.
27. St. Lawrence KS, Frank JA, McLaughlin AC. Effect of restricted water exchange rate on cerebral blood flow values calculated with arterial spin tagging: a theoretical investigation. Magn Reson Med 2000;44: 440–449.
28. Ye FQ, Mattay VS, Frank JA, Weinberger DR, McLaughlin AC. Comparison of white and grey matter transit times in spin tagging experiments. In: Proceedings of the 7th Annual Meeting of ISMRM, Philadelphia, 1999. p 1857.
29. Frackowiak RSJ, Lenzi G-L, Jones T, Heather JD. Quantitative measurement of regional cerebral blood flow and oxygen metabolism in man using ^{15}O and positron emission tomography: theory, procedure, and normal values. J Comput Assist Tomogr 1980;4:727–736.
30. Lammertsma AA, Frackowiak RSJ, Hoffman JM, Huang S-C, Weinberg IN, Dahlbom M, MacDonald NS, Hoffman EJ, Mazziotta JC, Heather JD, Forse GR, Phelps ME, Jones T. The $C^{15}O_2$ build-up technique to measure regional cerebral blood flow and volume of distribution of water. J Cereb Blood Flow Metab 1989;9:461–470.
31. Herscovitch P, Markham J, Raichle ME. Brain blood flow measured with intravenous $H_2{}^{15}O$. 1. Theory and error analysis. J Nucl Med 1983;24:782–789.
32. Koeppe RA, Hutchins GD, Rothley JM, Hichwa RD. Examination of assumptions for local cerebral blood flow studies in PET. J Nucl Med 1987;28:1695–1703.
33. Lammerstma AA, Jones T, Frackowiak RSJ, Lenzi G-L. A theoretical study of the steady-state model for measuring regional cerebral blood flow and oxygen utilization using oxygen-15. J Comput Assist Tomogr 1981;5:544–550.
34. Jones SC, Greenberg JH, Reivich M. Error analysis for the determination of cerebral blood flow with the continuous inhalation of ^{15}O-labeled carbon dioxide and positron emission tomography. J Comput Assist Tomogr 1982;6:116–124.